16TH EUROPEAN CONFERENCE ON EARTHQUAKE ENGINEERING THESSALONIKI 18 - 21 JUNE 2018

# TSUNAMI RISK FOR INSURANCE PORTFOLIOS IN JAPAN

Jochen WOESSNER[1], Rozita FAHARANI[2], Chesley WILLIAMS[3], Natanya PORTO[4], Manabu MASUDA[5], Erin DOLLARHIDE[6], Sreenivas BINGI[7]

## ABSTRACT

The tsunami following the 2011 Tohoku megathrust earthquake of magnitude 9.0 showed the potential for significant damage and loss relevant to the insurance industry. To date, however, the perception of tsunami risk as compared to earthquake shaking risk remains limited in the insurance industry due to few available probabilistic tsunami risk models for the industry. Tsunami is considered a secondary peril to an earthquake model but requires large computational resources as it is a high-resolution peril as inundation and tsunami wave runup need to be calculated at high resolution. We therefore present the probabilistic tsunami model methodology that addresses these issues and is included in the 2018 RMS HD earthquake model for Japan.
Based on the stochastic events of offshore earthquakes, we generate non-uniform finite fault slip models for events of $M_W \geq 7.5$. Computed elastic seafloor/coastline deformations, peak slip and location of slip patches constrain the selection of slip models to match observations and expected variations. The deformations serve as initial conditions to the high-resolution numerical modeling of tsunami wave propagation and coastal inundations solving the non-linear shallow water equation. Variable land surface roughness based on land cover data is used to simulate accurate hydraulics of coastal inundation.
Our results are based on the source geometries of the 2017 Japanese seismic hazard model. Inundation and tsunami runup results are compatible with measurements of the 2011 Tohoku earthquake and tsunami. The presented mean damage ratio patterns illustrate the high-resolution capabilities of the RMS tsunami model as basis for economic loss assessment.

*Keywords: Probabilistic tsunami risk assessment; Source Complexity; Inundation maps; Japan*

## 1. INTRODUCTION

Tsunami hazard and risk is generally considered a tail risk across the insurance industry. Infrequent mega-thrust subduction events are the major contributors to tsunami hazard and risk whereas ground shaking hazard and risk have a more diverse set of predominantly contributing earthquake sources. In the case of Japan, a substantial portion of exposure is situated close to the coastline roughly within the first ten kilometers of the coast. This specific distribution increases the ratio of tsunami risk to earthquake risk in comparison to many other countries across the world. Japan is thus a prime object for developing and learning about the interplay of earthquake and earthquake induced tsunami loss estimations.
Over the last years, RMS systematically improved tsunami hazard assessment for the insurance industry, starting from scenario based approaches, to applying empirical based inundation assessment, to developing a global tsunami catalog for local and long-distance tsunami hazard assessment. Recently, the development focused on a comprehensive probabilistic tsunami hazard assessment

[1]Lead Modeler, Risk Management Solutions Inc., Zurich, Switzerland, jochen.woessner@rms.com
[2]Senior Modeler, Risk Management Solutions Inc., Newark, USA, rozita.farahani@rms.com
[3]Sen. Director, Risk Management Solutions Inc., Newark, USA, chesley.williams@rms.com
[4]Lead Modeler, Risk Management Solutions Inc., Newark, USA, natanya.porto@rms.com
[5]Sen. Director, Risk Management Solutions Inc., Newark, USA, manabu.masuda@rms.com
[6]Sen. Product Manager, Risk Management Solutions Inc., Newark, USA, erin.dollarhide@rms.com
[7]Manager, Risk Management Solutions Inc., Newark, USA, sreenivas.bingi@rms.com

(PTHA) for local tsunami sources. The innovation for the insurance industry is a deeply science-based perspective on tsunami risk embracing the uncertainty in tsunami generation due to the variability of possible rupture scenarios on causative offshore faults and subduction interfaces. The rupture variability is integrated statistically by non-uniform slip distributions, or more correctly, finite fault slip distributions. To date, we limit the input to tsunami generation to the final slip distribution, acknowledging however that the temporal evolution of slip on the rupture plane can play a strong role when the initial tsunami waves are generated (Goda et al., 2017).

In this application for Japan, we develop a risk-targeted PTHA utilizing the defined sources as provided by the Headquarters for Earthquake Research Promotion (HERP). For each source hosting $M_W \geq 7.5$ events, a set of non-uniform slip distributions for subduction interface and intraslab sources along the Nankai trough, the Sagami trough, and the Japan trench along the Japanese east coast are generated. The set of sources also includes events along the outer rise of the Japan trench and in the Japanese sea as defined in the National Seismic Hazard project 2017. The fault surfaces are discretized using Delaunay triangulation and a triangular elastic dislocation model is used to model the seafloor/coastline uplift and subsidence. The seafloor/coastline deformations are input to a high-resolution numerical model to calculate the tsunami wave propagation and coastal inundations. Tsunami inundation and hazard maps are developed for the entire coast of Japan and are convolved with the RMS exposure, vulnerability and financial model to calculated mean damage ratios and economic losses.

We provide details about the earthquake sources generation, the deformation modeling, inundation maps and mean damage ratios and explain the performance of the approach by comparisons in particular to the observed data of the 2011 Tohoku data, putting the work in perspective to similar works for Japan.

## 2. METHOD

Probabilistic Tsunami Hazard Assessment combines, similar to Probabilistic Seismic Hazard Assessment (PSHA), a set of individual components that are essential to estimate exceedance probabilities of an intensity parameter within a given time frame, such as exceedance probabilities of tsunami runup heights or maximum inundation levels within a given period. In short, there are four major components to generate a PTHA (Figure 1):

1. Prepare an earthquake source model that defines the fault geometries, the magnitudes, and the annual rate of occurrence of the events;
2. Prepare an earthquake rupture model that defines how, for a given fault geometry and magnitude the slip is distributed across the fault plane;
3. Calculate the (elastic) dislocation in the study area and in particular across the rupture area as input for the initial tsunami wave calculation
4. Model the tsunami wave propagation across the sea, tsunami runup and inundation on the coast.
5. Combine the inundation results with the exposure, vulnerability, and financial model to estimate financial losses.

Each of these components has its range of possible solutions, in particular, the definition of earthquake sources is non-unique and needs to be treated in a probabilistic sense.

The RMS tsunami modeling strategy has evolved over the recent years to move from a scenario based approach to a probabilistic approach. While the first models were including a limited set of sources and solutions, the tsunami model for Japan now includes a comprehensive yet not exhaustive set of tsunami solutions with a specific focus on modelling the variability of possible slip distributions.

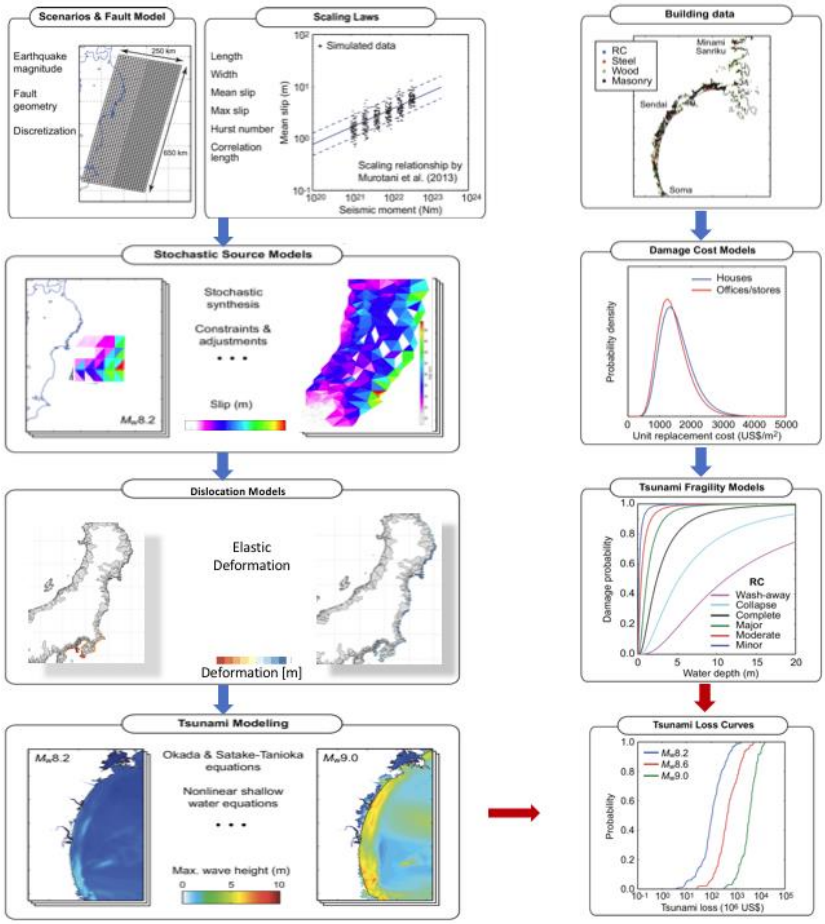


Figure 1. Schematic procedure for a Probabilistic Tsunami Hazard Assessment (PTHA). Figure adapted and modified from (Goda and Abilova, 2016).

### *2.1 Source and Deformation Modeling*

Earthquake ruptures along faults in the oceanic crust can cause significant vertical and lateral displacement of the ocean floor. These ruptures are located on the primary interface, however, the rupture can potentially continue/trigger ruptures on splay faults in the accretion wedge in the continental plate above the subducting interface. In general, thrust events are generating tsunamis, however, normal faulting events in the outer rise of the subduction plate can also cause tsunamis.
Recent studies have shown that fault geometry and details of the slip distribution have significant impact on initial tsunami wave heights, run-up and inundation along the coastal areas, besides the influence and effects of the bathymetry, topography, friction and so on (Davies et al. 2015, Goda et al. 2014, Horspool et al. 2014, LeVeque et al. 2016, Melgar et al. 2016, Selva et al. 2016, Wang et al. 2013, Witter et al. 2011).
Based on this evidence, RMS uses the following steps to model ruptures of earthquakes:

1) Define triangulated surface from the event geometry,
2) Model a set of finite fault slip distributions,
3) Calculate deformation along coastline and in the source region,
4) Select events according to maximum slip, location of slip on rupture plane, deformation along coastline and in source region.

The spatial complexity of slip, albeit being unquestionable, is physically not entirely understood. The finite-fault slip models reveal many features that, however, can be described stochastically. Several methods have been proposed to characterize the heterogeneous nature of fault slip (Mai and Beroza 2002, Somerville et al. 1999). The method by Mai and Beroza (2002) has found the most applications: as basis to simulate ground motions, for testing correlations of slip and stress patterns along faults (Woessner et al., 2006), and most importantly here to characterize slip distributions for great

earthquakes, such as the Tohoku 2011 M9-type event (Goda 2015, Goda et al. 2014). The ideas of Mai and Beroza (2002) have been further developed to generate static slip generation on arbitrarily complex faults using the Karhunen-Loève expansion (LeVeque et al., 2016). This has been expanded and tested for Cascadia subduction events (Melgar et al., 2016).

We apply the approach proposed by Melgar et al. (2016) to account for the complex structure of the subduction interfaces along the eastern coast of Japan. While we believe that other method are similarly viable (Goda et al., 2017), our choice considers the synchronized use of triangulated surfaces for slip modeling and elastic dislocation calculation (Meade, 2007). Details of the slip model generation method are outlined in Melgar et al. (2016). In the next paragraphs, we focus on the implementation steps to set up a comprehensive set of tsunami sources.

The geometry and magnitudes of the tsunami sources are derived from the set of sources (Figure 2) that are provided by HERP through the Japan Seismic Hazard Information Stations (http://www.j-shis.bosai.go.jp/map/JSHIS2/download.html?lang=en). The sources are assigned a moment magnitude as used in the HERP seismic hazard model which we enhanced by adding simple magnitude uncertainty with $M_W \pm 0.1$ and $M_W \pm 0.2$ and a weighting scheme with weight of 0.1, 0.2 and 0.4 to sample uncertainties. Thereafter, between 100-500 finite fault slip models are generated. While all these models are viable solutions, not all of those models are either physically possible nor are all prone to generate tsunamis. The method primarily preserves the stochastic properties of the distribution of slip patches, while it does not consider physical constraints. The stochastic properties constrain the ratio of patches with small slip values to patches with large slip values and their spatial correlation.

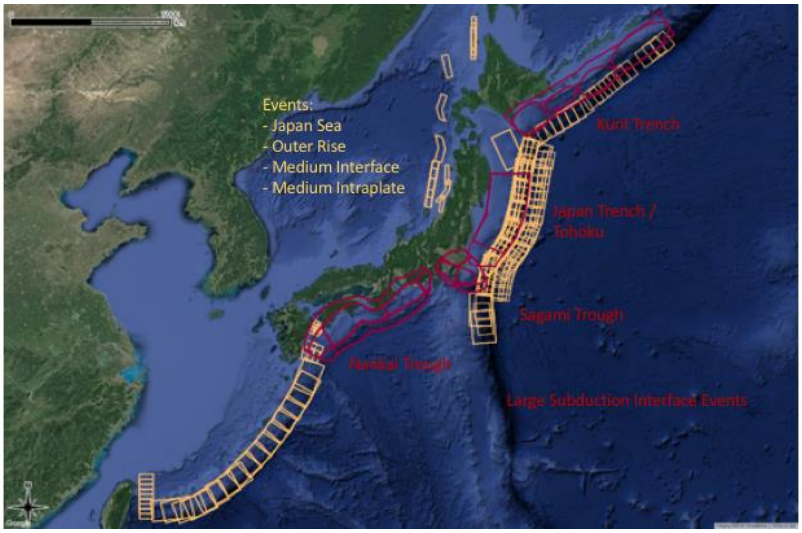


Figure 2. Location of tsunamogenic earthquake sources for the RMS Japan PTHA model. Colours differentiate large subduction interface events (red) and other offshore events that are assumed to generate tsunamis (yellow).

It is therefore necessary to define a set of criteria to ensure that the ruptures generate a tsunami. These criteria need to consider the size and distribution of slip, but also resulting deformation. Thus, for each slip model, the elastic deformation of the seafloor in the source area and along the Japanese coastline is calculated. Slip models are then selected using a combination of criteria on the maximum slip, location of slip on rupture plane, deformation along the coastline and in the source region. For example, the maximum slip on the fault plane depends on the event magnitude; RMS uses a limit for maximum slip of M9-type events constrained to 55m not to generate unrealistic initial tsunami waves. Subsidence and uplift along the coastline is limited to a range of ±10 meters for the largest events on the Nankai trough where independent terrace uplift data is able to constrain this, however, for events such as the Tohoku 2011 event that occur on the Japan trench, these limits are smaller as the subduction interface is at larger distances to the coastline. In terms of slip distribution, more than two-thirds of the total slip is required to occur in the upper section of the fault plane. Given the assumption that only events with $M_W \geq 7.5$ generate tsunamis considered to be significant also in terms of losses as

well as the number of sources defined by the 2017 National seismic hazard map, 766 tsunamis are considered in this tsunami hazard assessment.
It is important to note the difference between a general risk-targeted tsunami model and a risk-targeted tsunami model for the insurance industry. The latter starts from a stochastic event set optimized to accurately assess risk given the country-wide exposure distribution, population density can be considered a proxy for this. Thus the total rate, also for the entire earthquake rate set, is reduced as non-loss causing earthquake and earthquake induced tsunamis are not considered. The interest is focused on events and tsunamis that cause substantial economic loss. Therefore, tsunamis in this manuscript are defined as tsunamis that cause substantial economic losses.
Earthquakes that generate tsunamis causing substantial losses in addition to those generated from ground shaking are certainly less frequent than earthquakes that generate loss by ground shaking only. In our model, this is visible in the cumulative frequency magnitude distribution when selecting the rates of those events that cause a tsunami (Figure 3, blue line, TI Tsunami) as compared to when not (Figure 3, red line, TI ALL). The TI ALL curve is the rate for the time-independent RMS model of all stochastic events with events not causing ground shaking based economic losses removed; thus the rate is smaller when compared to any version of the earthquake catalog provided by the Japanese Meteorological Agency (declustered or not). From Figure 3, it is also evident that the percentage of $M_W$ =7.5 type events are less likely to generate a loss causing tsunami as compared to an $M_W$ =8.4 type event. The RMS model includes the assumption that all offshore events with $M_W \geq 8.6$ cause significant loss which is why the two curves then overlay.
In terms of average return periods, earthquakes with $M_W \geq 7.5$ occur about every 2.3years, while loss causing tsunamis due to events with $M_W \geq 7.5$ occur every 15.3 years on average. For $M_W \geq 8$ these recurrence periods are 9.0y vs. 24.2y and for $M_W \geq 8.5$ these are 98.9y vs 114.8y. For $M_W \geq 8.6$, this equals out as designed in our model definition.

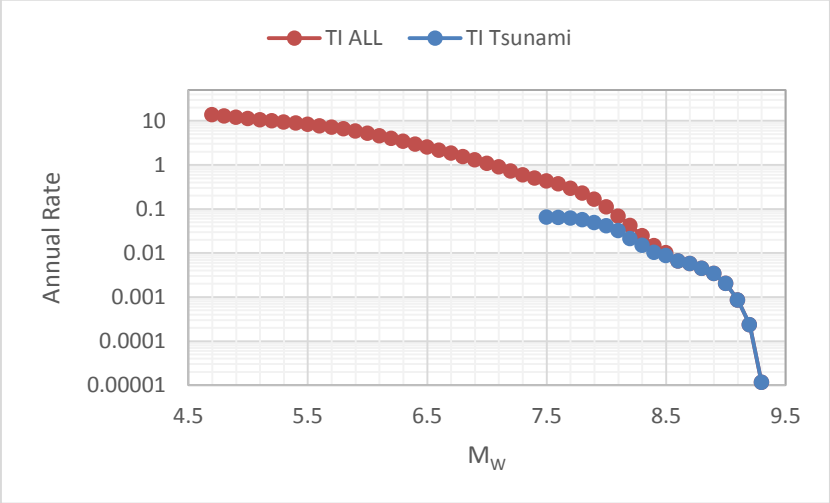


Figure 3. Cumulative magnitude frequency distribution of the RMS Japan time-independent model for tsunami generating events (TI Tsunami, blue) and entire earthquake model (TI ALL, red).

Figure 4 displays three solutions for an M9 type earthquake on the Tohoku source as defined by HERP. The non-uniform slip distributions display a variety of possible scenarios with high-slip concentrations to the south, in the center or to the north. Deformation just on top of the rupture plane reach slightly more than 12m, generating initial water column uplift of about the same level. Subsidence along the coast reach peak values above 5m which is larger than what has been observed in the GPS-observations of the 2011 Tohoku event. It needs to be noted that the purely elastic deformation may overestimate the actual measured deformation values as crustal deformation is not acting purely elastically and thus deformation tends to be smaller in reality.

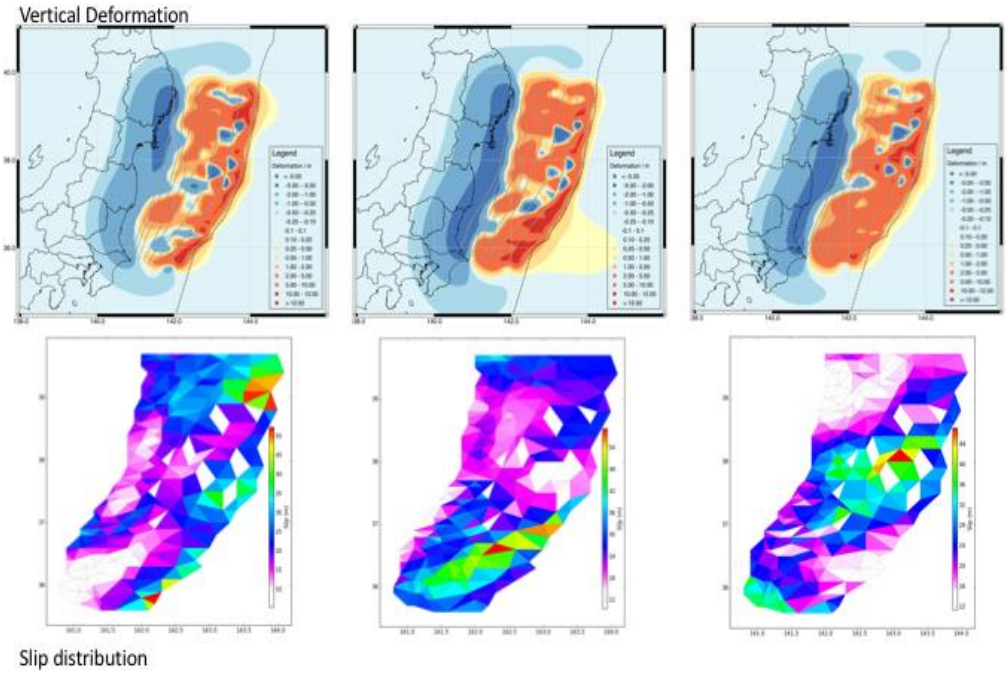


Figure 4. (Bottom row) Scenario slip distributions for the M9-type Tohoku sources. (Top row) Vertical elastic deformation pattern corresponding to the slip distributions below.

### *2.2 Tsunami Modeling*

#### *2.2.1 Wave Model*

Hydrodynamic characteristics of tsunami waves are influenced by the initial tsunami waveforms as well as the surrounding bathymetric and topographic profiles. To accurately model the variations of tsunami height and length during wave propagation and coastal inundation, we solve the nonlinear shallow water equations using finite volume numerical method. To accelerate the comprehensive computational efforts, parallel computation on Graphic Processing Units (GPUs) was implemented.
Three levels of nested grids with different resolutions are used to perform the numerical modeling and capture the coastal processes including wave reflection, diffraction, and refraction: Great Japan Grid of relatively coarse (~1km) resolution (Low resolution grid), 15 grids of intermediate (~450m) resolution (intermediate grid), and 118 grids of fine (~50m) resolution (High resolution grid). The great Japan grid (low resolution grid) of ~1km grid is derived from GEBCO, 2014 gridded bathymetric data sets that include global terrain models for ocean and land (Sandwell et al. 2002). 15 grids of intermediate (~450m) resolution and 118 grids of fine (~50m) resolution are resampled from Japan Cabinet Office elevation data (source: Japan Cabinet Office). The grids and the model output of wave elevations are referenced to mean sea level.
The bathymetric/topographic computational grids are adjusted for each of the 766 stochastic tsunamogenic earthquakes to account for the seafloor/land deformation. For each event, the fault surface is discretized by Delaunay triangles and the initial deformation of seafloor and coastal land is computed using the triangular dislocation model (Meade, 2007). Then the vertical deformation values (including subsidence and uplift) are added to the bathymetric and topographic elevation values. The low resolution, intermediate, and high resolution grids interact with each other by passing boundary conditions between nodes along the intersecting boundaries. At the grid boundaries, wave heights as well as wave fluxes in horizontal directions (x and y) are used as the boundary conditions. The low resolution grid passes data to the intermediate grids and the intermediate grids pass data to the high resolution grids. As the wave travels to shallower water, the resolution of grids become finer to accurately model the shorter wavelengths. For all the grids, both land and ocean is considered in the numerical simulations to account for the complicated wave dynamics, refraction, diffraction, wave reflection, and other coastal processes.

The initial sea surface displacement at the time of tsunami generation (initial tsunami wave) is assumed to be identical to the seafloor/land deformation. To consider land friction in the hydrodynamic modeling of wave run-up and coastal inundation, variable surface roughness is considered in the wave model. The existence of vegetation or man-made structures alerts the amount and pattern of tsunami inundation. Therefore, it is important to consider the variable surface roughness based on the land cover data. For this purpose Global Land Use Land Cover (LULC) is used and resampled for the fine resolution grids. For the intermediate grids the roughness data provided by Cabinet office is used.
The numerical model is run for 6 hours after the generation of the tsunami waves to model the full lifetime of tsunami waves, coastal processes, and coastal inundation.

*2.2.2 Historical 2011 tsunami event*

The $M_W$ =9.1 2011 Tohoku earthquake and tsunami occurred at 14:46 JST on Friday 11 March 2011. The earthquake ground shaking and the tsunami waves impacted northeast coast of Japan as well as the far-field regions. They travelled along the Pacific Ocean and reached Crescent city in USA.
A lot of studies have been done regarding the reconstruction of slip distribution of Tohoku event. In this study we used Simons et all, 2011 who used GPS satellite data to calculate slip values and slip distribution in this event.
For validation purposes, we compare the numerical results of water elevation in inundated areas with observation data (Figure 5). Tsunami waves are travelling from right of the image to the left. Numerical results are shown in solid color and the observation data is shown in circles. As shown in this figure numerical results agree very well with the observation data in terms of inundation extent as well as the water elevations.
In addition, we performed a study on the maximum wave runup and compared it with the casualty data gathered by UNESCO (Figure 6). Ishinomaki in Miyagi Prefecture experiences the highest runup of about 20m. At the same location about 4000 people were reported to be dead or missing. This comparison shows that the real-time numerical results of runup can be used in future to predict the most vulnerable regions to that specific tsunami. The results can be used by warning systems as well as the first responders who would go to the most vulnerable regions after a disaster occurs. In our stochastic set 10 out of 766 events for the Tohoku source with a variety of possible slip distribution ( Figure 4). Results will be presented in the next sections.

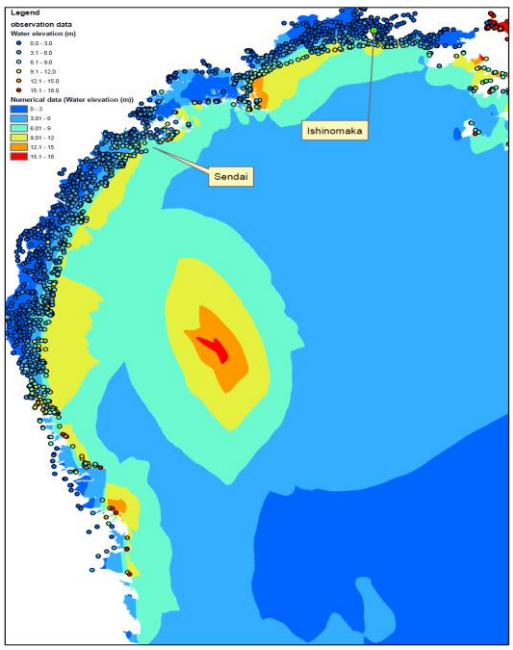


Figure 5. Comparison of numerical result of water elevation for 2011 Tohoku event with observation data (solid color is corresponding to numerical results, circles are corresponding to observation data)

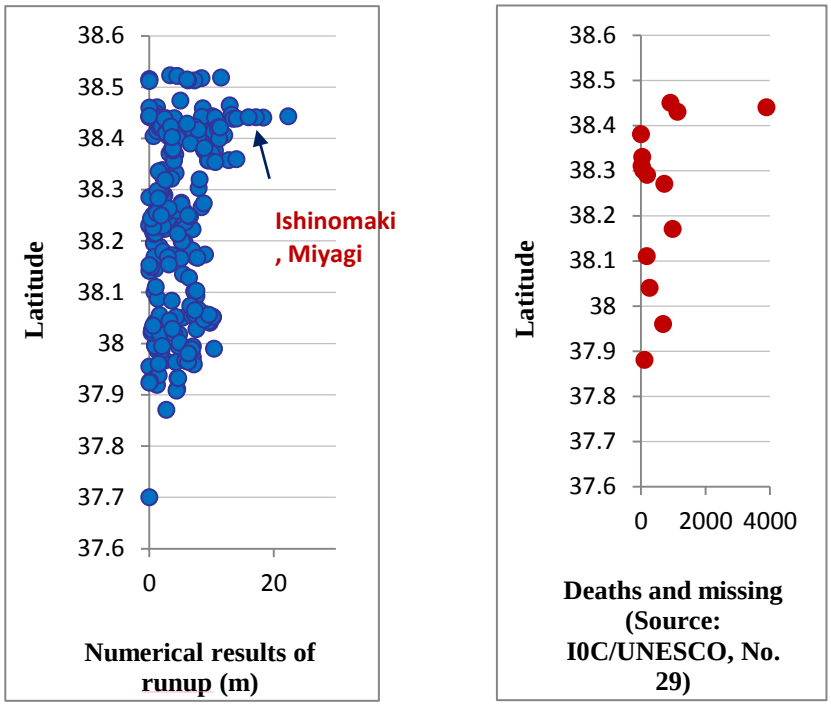


Figure 6. Runup simulations (left) and reported deaths and missing in Sendai region (right).

*2.2.3 Inundation Results*

The numerical wave model is used to model the tsunami wave propagation and coastal inundation for each stochastic tsunami event along the Japanese coastline. GPU parallel computation is used to accelerate the high computational efforts needed to solve wave equations on three layers of embedded grids. Tsunami hazard maps including the inundation depths and tsunami extends are developed.
Figure 7 shows the histogram of maximum water depth at Tokyo and Chiba cities. The histograms include results of 87 tsunami events out of 766 stochastic events, which were generated on the Sagami Trough geometries (not shown). These examples are chosen as the Sagami Trough events is often considered as primary tsunami source for the Tokyo area. Tokyo could experience a maximum of water depth of 3m, while Chiba city could experience water depth up to 5m. Tokyo and Chiba are geographically close to each other, however, the geographic and bathymetric profile of coastline as well as the direction of generated tsunami waves, make Chiba more vulnerable to tsunami waves in comparison to Tokyo city.
Figure 8 shows an inundation map of one of our stochastic events at Sendai region as well as the histogram of maximum water depth at Ishinomaki and Sendai cities. The histograms include results of 10 tsunamis out of 766, which were generated at HERP Tohoku rupture zone. These 10 events are using the HERP Tohoku source that extend slightly further to the south as the 2011 Tohoku source event but with different slip realizations (see Figure 4). As shown in Figure 6, these events have high impact on Ishinomaki and Sendai cities. The maximum water depth could reach ~16m in Ishinomaki city and ~14m in Sendai city. Ishinomaki experiences higher tsunami waves in comparison to the Sendai city due to the direction of how propagate towards the two cities. The largest coastal inundations correlates to the height of initial seafloor uplift, which generates the initial tsunami waves but other parameters such as bathymetry and topography profiles and characteristics of land cover could play an important role in the wave heights, wave lengths and their directions. In addition, coastal processes such as secondary waves, reflected waves, wave refraction and wave diffraction play an important role in the extends of tsunami inundations.

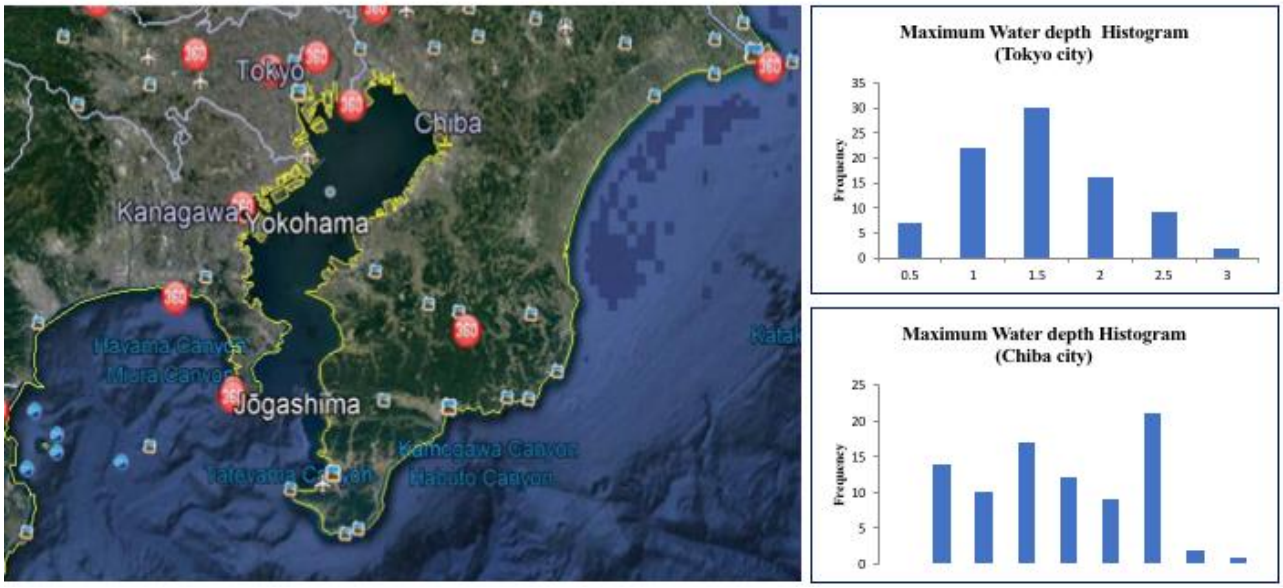


Figure 7. Histogram of maximum water depth (m) at Tokyo and Chiba cities. Note: Only tsunami events generated from Sagami trough are included in these histograms (87 Sagami ruptures).

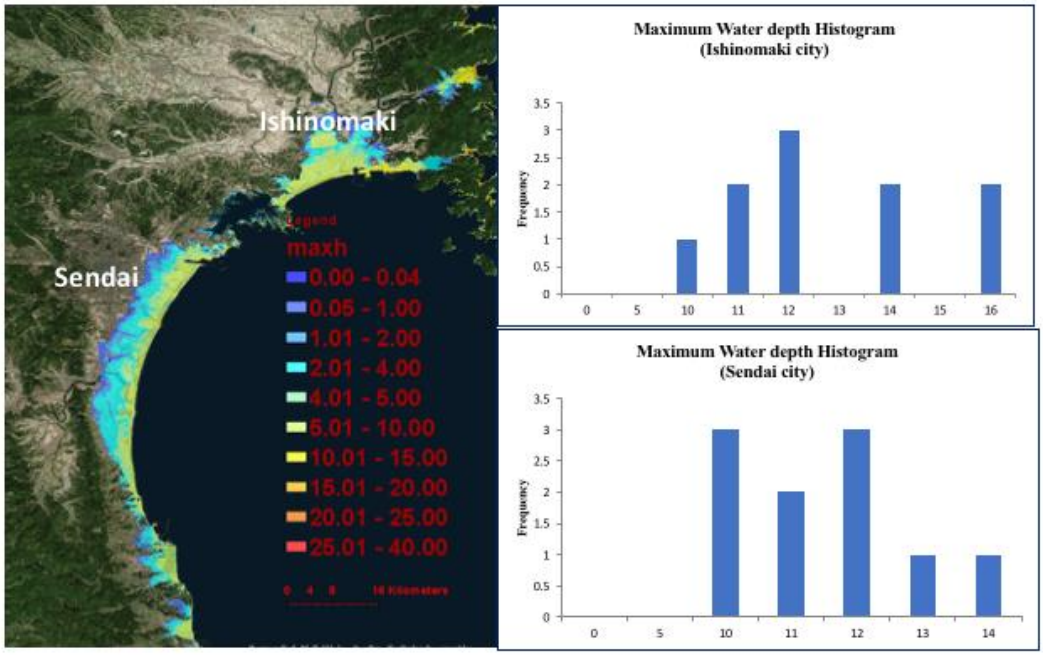


Figure 8. (Left) Inundation depths and extent at Sendai region corresponding to one of stochastic events. (Top right) Histogram of maximum water depth (m) at Ishinomaki and (Bottom right) Sendai cities. Note: Only 10 tsunamis generated from Tohoku rupture zone as in HERP are included in these histograms .

Figure 9 illustrates an inundation map of one of our stochastic events at Fukushima nuclear plant region as well as the histogram of maximum water depth at Fukushima Daiichi plant and Fukushima Daini plant. The histograms include the 10 HERP Tohoku tsunami source events and have very high inundations on both locations, the Daiichi and Daini nuclear plants. The maximum water depth reaches up to ~24m at both of these nuclear plants illustrating their high risk related to tsunami waves generated from the Tohoku rupture zone. The Daiichi plant suffered from fatal damage following the 2011 tsunami and several reactors of Daini nuclear plant automatically shut down.

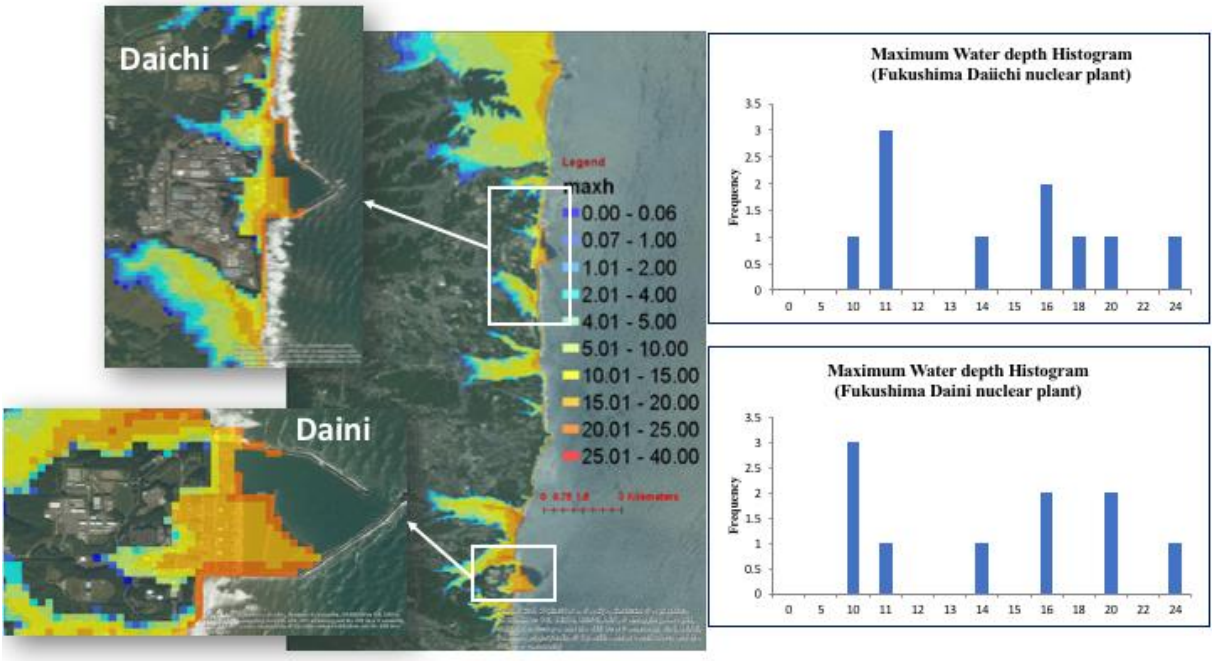


Figure 9. (Left) Inundation depths and extent at Fukushima region corresponding to one of HERP Tohoku source stochastic events. (Right top) Histogram of maximum water depth (m) at Fukushima Daiichi nuclear plant and (Right bottom) Fukushima Daini nuclear plant. Note: Only tsunami events generated from HERP Tohoku rupture zone are included in these histograms (10 events are generated from the tsunami rupture).

## 3. ECONOMIC TSUNAMI RISK

Large tsunamis can results in large economic and insured losses for local communities as well as for the global community due to the business interruption. In addition to the tsunami hazard model that includes tsunami generation, wave propagation, and coastal inundation, RMS has developed a tsunami vulnerability model that identifies the vulnerability of buildings and onshore structures to the tsunami waves in different regions. The tsunami vulnerability model includes an extensive empirical analysis that was developed using the detailed tsunami damage data of 2011 Tohoku event (Charvet et al. 2015, Farahani et al. 2017, Masuda et al. 2012). The tsunami hazard model and the vulnerability model are combined by the exposure model to deliver economic losses.

Figure 10 illustrates the inundation map of one of the Tohoku-like stochastic events along with the corresponding Mean Damage Ratio (MDR) values. Regions with high inundation depths result in MDR values close to 100% MDR imply fatal damage of structures. Mean Damage Ratios (MDR) are calculated by the convolution of the vulnerability with the hazard values. The calculations are performed on 50m resolution grids and for each $50m^2$ cell, an MDR-value is calculated for each of the stochastic events leading to a range of possible outcomes depending on the rupture scenario. The inundation map MDR comparison shows the impact of the inundation height with the MDR in each cell, illustrating also that higher inundation values lead to higher MDRs.

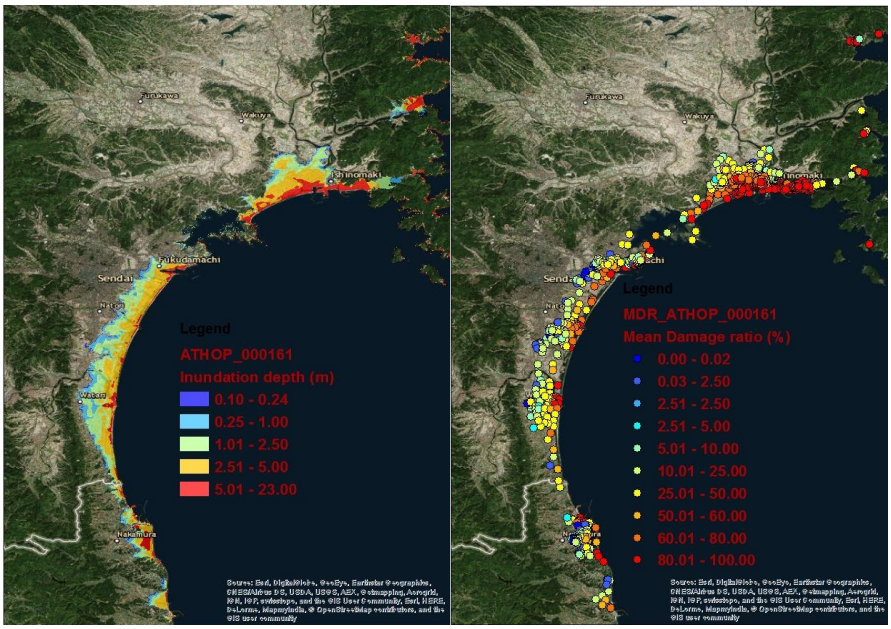


Figure 10. Left: Inundation map of one of the stochastic tsunami event. Right: Corresponding Mean Damage Ratios (MDR)

## 4. CONCLUSIONS

We implemented a comprehensive probabilistic method to model tsunami risk for insurance portfolios across Japan. We detail the methodology for the probabilistic tsunami model based on the source geometry definition and various non-uniform slip-distributions, calculated and selected for the offshore sources as defined in the 2017 National seismic hazard map for Japan. We compare and evaluate the modeling steps to data observed following the 2011 Tohoku M9-type event.
We reconstructed the 2011 Tohoku tsunami event and compared the modeled runup with the observed data to validate the numerical model achieving good qualitative and quantitative agreement. Then we numerically modeled the tsunami waves generated from the full set of probabilistic non-uniform slip-distributions. Histograms of inundation values illustrate the impact on various key cities and locations of Japan. The distribution of mean damage ratios highlights their correlation with the inundation maps and also illustrates the RMS model capability to resolve local damage differences at a scale of $50m^2$ along the coastlines of Japan. The mean damage ratios serve to estimate and differentiate economic risk at various administrative divisions relevant for the financial industry in Japan.

## 5. REFERENCES

Charvet I, Suppasri A, et al. (2015). A multivariate generalized linear tsunami fragility model for Kesennuma City based on maximum flow depths, velocities and debris impact, with evaluation of predictive accuracy. Natural Hazards, 79(3): 2073–2099, https://doi.org/10.1007/s11069-015-1947-8.

Davies G, Horspool N, et al. (2015). Tsunami inundation from heterogeneous earthquake slip distributions: Evaluation of synthetic source models. Journal of Geophysical Research: Solid Earth, https://doi.org/10.1002/2015JB012272.

Farahani RJ, Woessner J, et al. (2017). Tsunami Risk for insurance portfolios from mgathrust earthquakes in the Cascadia subduction zone. In 16th World Conference on Earthquake Engineering (p. Paper No 3149). Santiago de Chile.

Goda K (2015). Effects of Seabed Surface Rupture Versus Buried Rupture on Tsunami Wave Modeling: A Case Study for the 2011 Tohoku, Japan, Earthquake. Bulletin of the Seismological Society of America, 105(5): 2563–2571, https://doi.org/10.1785/0120150091.

Goda K, Abilova K (2016). Tsunami hazard warning and risk prediction based on inaccurate earthquake source parameters. Natural Hazards and Earth System Sciences, 16(2): 577–593, https://doi.org/10.5194/nhess-16-577-2016.

Goda K, Mai P, et al. (2014). Sensitivity of tsunami wave profiles and inundation simulations to earthquake slip and fault geometry for the 2011 Tohoku earthquake. Earth, Planets and Space, 66(1), 105, https://doi.org/10.1186/1880-5981-66-105.

Goda K, Yasuda T, et al. (2017). Tsunami simulations of mega-thrust earthquakes in the Nankai–Tonankai Trough (Japan) based on stochastic rupture scenarios. Geological Society, London, Special Publications, SP456.1. https://doi.org/10.1144/SP456.1.

Horspool N, Pranantyo I, et al. (2014). A probabilistic tsunami hazard assessment for Indonesia. Natural Hazards and Earth System Science, 14(11): 3105–3122. https://doi.org/10.5194/nhess-14-3105-2014.

LeVeque RJ, Waagan K, et al. (2016). Generating Random Earthquake Events for Probabilistic Tsunami Hazard Assessment. Pure and Applied Geophysics, https://doi.org/10.1007/s00024-016-1357-1.

Mai, PM, Beroza GC (2002). A spatial random field model to characterize complexity in earthquake slip. J. Geophys. Res., 107(B11). https://doi.org/10.1029/201JB000588.

Masuda M, Williams C, et al. (2012). Tsunami vulnerability function development based on the 2011 Tohoku earthquake in Japan. In Proceedings of the 15th World Conference on Earthquake Engineering. Lisbon.

Meade BJ (2007). Algorithms for the calculation of exact displacements, strains, and stresses for triangular dislocation elements in a uniform elastic half space. Computers & Geosciences, 33(8): 1064–1075, https://doi.org/10.1016/j.cageo.2006.12.003.

Melgar D, LeVeque RJ,et al. (2016). Kinematic rupture scenarios and synthetic displacement data: An example application to the Cascadia subduction zone. Journal of Geophysical Research: Solid Earth, https://doi.org/10.1002/2016JB013314.

Sandwell DT, Gille ST, et al. (2002). Bathymetry from Space: Oceonography, Geophysics and Climate (D. T. Sandwell, S. T. Gille, & W. H. F. Smith, Eds.). Maryland: Geoscience Professional Services. Retrieved from https://www.geo-prose.com/pdfs/bathy_from_space.pdf.

Selva J, Tonini R (2016). Quantification of source uncertainties in Seismic Probabilistic Tsunami Hazard Analysis (SPTHA). Geophysical Journal International, 205(3): 1780–1803, https://doi.org/10.1093/gji/ggw107.

Somerville P, Irikura K, et al. (1999). Characterizing crustal earthquake slip models for the prediction of strong ground motion. Seism. Res. Let., 70(1): 59–80.

Wang PL, Engelhart, SE, et al. (2013). Heterogeneous rupture in the great Cascadia earthquake of 1700 inferred from coastal subsidence estimates. Journal of Geophysical Research: Solid Earth, 118(5): 2460–2473. https://doi.org/10.1002/jgrb.50101.

Witter R, Zhang Y, et al. (2011). Simulating tsunami inundation at Badon, Coos County, Oregon, using hypothetical Cascadia and Alaska earthquake scenarios. AGU Fall meeting 2011, NH16.

Woessner J, Schorlemmer D, et al. (2006). Spatial correlation of aftershock locations and on-fault main shock properties. Journal of Geophysical Research, 111(B8): B08301. https://doi.org/10.1029/2005JB003961.